Pressure Dependency of Elasticity in α-TiZr Shape Memory Alloys

Job W. Wafula,[1,2] George S. Manyali,[2] John W. Makokha,[1] James Sifuna [2,3,4]

[1]Materials Science, Department of Science, Technology and Engineering,
Kibabii University, 1699-50200, Bungoma, Kenya,

[2]Computational and Theoretical physics group (CTheP), Department of Physics,
Masinde Muliro University of Science and Technology, 190-50100, Kakamega, Kenya,

[3]Materials Modeling Group, Department of Physics and Space Sciences,
The Technical University of Kenya, 52428-00200, Nairobi, Kenya

[4]Department of Natural sciences,
The Catholic University of Eastern Africa, 62157-00200, Nairobi, Kenya

Tel: + 254715158787, + 254728317456, +254721825520, +254725499073
Email: jobwafula691@gmail.com, georgemanyali@mail.com, makokhajw@gmail.com, sifunajames@gmail.com.

Abstract:

Shape memory alloys are a group of materials with two noteworthy properties; shape memory effects and superelasticity thus they have attracted a number of industrial applications. Elasticity is the ability of a material to resume its normal shape after being stretched or compressed when the elastic limit is not exceeded. Titanium Nickel, copper-based and iron-based shape memory alloys are mostly applied in constructions sector but they face challenges of pressure dependency. To provide a solution, we investigated the pressure dependency of elasticity in α-TiZr shape memory alloy. Elastic constants, bulk modulus, Young modulus, shear modulus and Poisson's ratio of α-TiZr shape memory alloy were calculated at different pressure (0-10GPa) using Quantum ESPRESSO code with post-processing of the data done using Thermo_pw code. Projector augmented wave pseudo-potential with Generalized Gradient Approximations (GGA) within Perdew, Burke, and Ernzerhof (PBE) exchange-correlation functional was applied in this study. Elastic constants; C_{11}, C_{12}, C_{13} C_{33}, and C_{66} of α-TiZr shape memory alloy increase with pressure monotonically except C_{44} which slightly decrease linearly. Furthermore, Bulk modulus, Young's modulus shear modulus and Poison's ratio were also observed to increase with external pressure. This indicates that elasticity of α-TiZr shape memory alloy is improved when external force is exerted on crystal. The study of pressure dependency of elasticity in α-TiZr shape memory alloy provides information which may lead to adoption of this alloy in construction of intelligent reinforced concrete (IRC).

Keywords: α-TiZr, Elasticity, Density functional theory.

1. Introduction

The Shape memory alloys (SMAs) belong to a class of shape memory materials (SMMs), which have the ability to 'memorise' or retain their previous form when subjected to certain stimulus such as thermo-mechanical (Jani *et al*., 2014). The Titanium Zirconium (TiZr) shape memory alloy undergoes a reversible martensitic transformation from the hexagonal 'α' martensite to the cubic '*β*' austenite at the start temperature (*As*) of 871 K and the martensitic transformation with the start temperature (*Ms*) of 813 K (Li *et al*., 2011). Shape memory alloys have been fully utilized in a number of industries due to their benefits of superelasticity, shape memory effect and high damping

properties. Titanium Nickel, copper-based and Iron-based shape SMAs are among materials so far used in the construction of concrete of buildings and bridges. However, the alloys mentioned above have not been fully adopted in the construction sector due to limitations of temperature (Chang *et al*., 2016) and pressure dependent behaviors. This is besides their low martensitic transformation temperatures (Baloyi *et al*., 2018). Variation of external pressure can cause cracks on buildings and bridges making them unsafe for use. SMA wires were introduced in civil structures as Intelligent Reinforced Concrete (IRC) because they can sense cracks and reduce large scale sized cracks. Therefore, there is need for building and bridge materials that can dissipate energy with minimum structural damage and return to their initial position as a result of changes in temperatures and pressures (Chancellor *et al*., 2014). The first application of SMAs in concrete structure was on a highway bridge in Michigan and from that innovative project that helped to close the cracks it was realized that the behavior of SMAs was to be under different working temperatures (Soroushian *et al*., 2015). The elastic properties of hexagonal crystal of TiZr SMA under the external pressure between 0 GPa to 10 GPa at constant temperature 0 K were investigated by the density functional theory method (DFT). This paper is organized as follows; in Section 2, the computation details are given. The results and discussion are presented in section 3. Finally, a conclusion of our results is shown in section 4.

2. Computational details

All the calculations were performed by Density Functional Theory (DFT) (Kohn *et al*., 1965) implemented in Quantum ESPRESSO codes (Giannozi *et al*., 2017) using Thermo_pw code as post-processing tool (Corso *et al*., 2016). The ion–electron interaction was described by the Projector augmented wave (PAW) method and exchange-correlation functional is treated within the Perdew, Burke, and Ernzerhof (PBE) of generalized gradient approximation (GGA) (Perdew *et al*., 1996). The valence electron configurations for Ti and Zr are $3d^3 4s^1$ and $4d^3 5s^1$. The plane wave cut-off energy was set as 50 Ry since it was sufficient to converge the total energy of α-TiZr Shape Memory Alloy. K-point meshes of 16×16×12 for the Brillouin zone was sampled based on Monkhorst-Pack scheme (Monkhorst *et al*., 1976). Before calculating the elastic constants of the TiZr alloy at a given pressure P, the unit cell of the compound at the corresponding pressure was relaxed until the atomic forces were less than 0.001 eV/Å and stress of less than 0.02 kbar.

3. Results and discussions

3.1 Structural properties

The unit cell of α-TiZr shape memory alloy in α structure consists of two atoms with space group P $\bar{6}$m2 (187) as shown in figure 1. Since the structure is hexagonal therefore lattice parameters; a=b≠c with bond angles $\alpha=\beta=90^0$ and $\gamma=120^0$ and the bond lengths under different pressure are presented in table 1. The α-TiZr shape memory alloy has sigma covalent bond with the mass of unit cell of 139.0910 a.m.u. The calculated values for lattice constants and bulk modulus both from Equation of state (EOS) and Thermo_pw tool presented in Table I are in good agreement with previous experimental and theoretical data at 0GPa.

 Available online http://ir.kabarak.ac.ke/handle/123456789/1

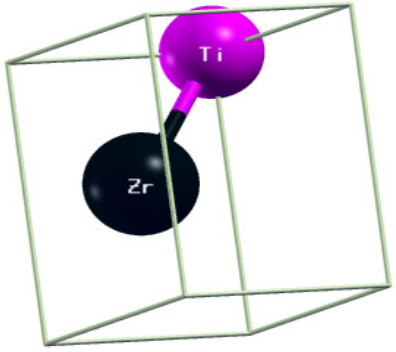

Figure 1. (Color online) The unit cell of α-TiZr with two atoms at Zr (0.333333 0.666667 0.250000) and Ti (0.666667 0.333333 0.750000) positions.

Table 1. Indicating the calculated values of the lattice parameter a, Bulk modulus B_0, the first pressure derivative of the Bulk modulus B', Bond length (Å) and the densities at different pressures in comparison with experimental studies and other theoretical work

Pressure (GPa)		Reference	a (Å)	B_0 (GPa)	B_o'	Bond length(Å)	Density(g/cm^3)
0	EOS	This work	3.08	97.73	3.42		5.62
0	Thermo_pw	This work	3.07			3.07	5.65
2			3.05			3.05	5.76
4			3.03			3.03	5.87
6			3.01			3.02	5.93
8			2.99			3.00	6.07
10			2.97			2.99	6.16
0	Expt	(Bashkin *et al.*, 2003)	3.10	148.00	3.80		
		(Li *et al.*, 2011)	3.12				
0	Other studies	(Wang *et al.*, 2011)	3.11	97.80	3.47		
		(ikehata *et al.*, 2004)	3.11				
		(Ho *et al.*, 2008)	3.06				

The bulk modulus and its pressure derivative were calculated by minimizing the total energy for different values of the lattice constant according to the third-order Birch–Murnaghan equation of state (EOS) (Birch, 1947).

$$P(V) = \frac{3B_0}{2}\left[\left(\frac{V_0}{V}\right)^{\frac{7}{3}} - \left(\frac{V_0}{V}\right)^{\frac{5}{3}}\right]\left\{1 + \frac{3}{4}(B_0' - 4)\left[\left(\frac{V_0}{V}\right)^{\frac{2}{3}} - 1\right]\right\} \quad (1)$$

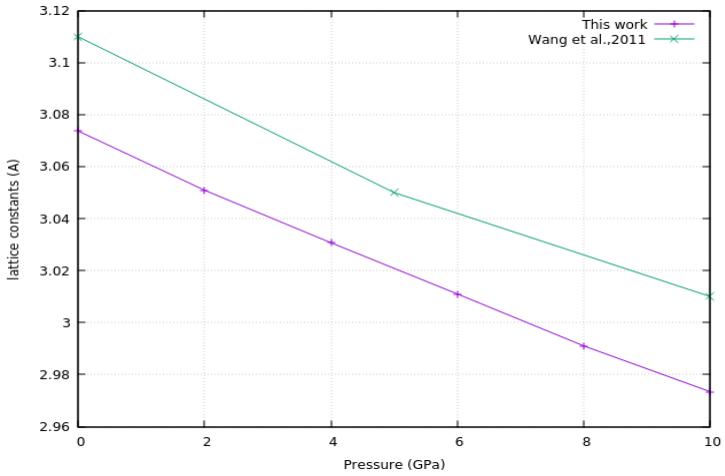

Figure 2. Calculated lattice parameters of α-TiZr Shape Memory Alloy under pressure in comparison with other theoretical data of Wang et al.

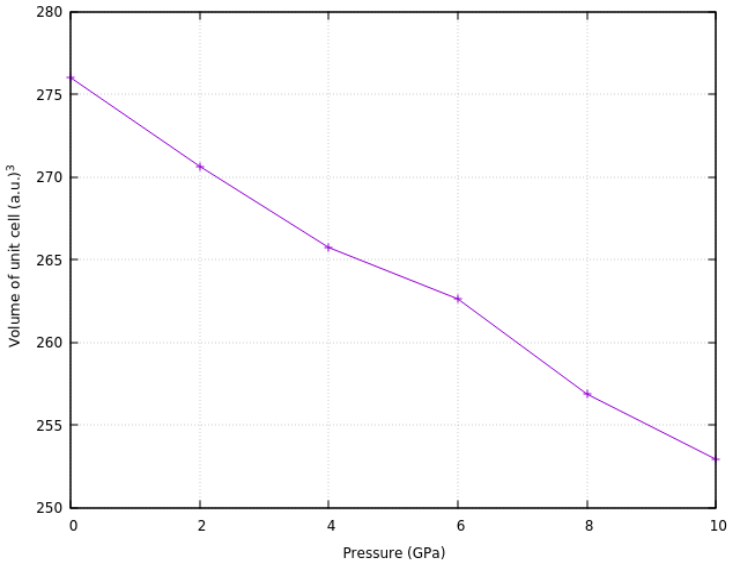

Figure 3. Shows the variation of volume of unit cell $(a.u)^3$ of α TiZr Shape memory alloy under external pressure up to 10GPa.

 Available online http://ir.kabarak.ac.ke/handle/123456789/1

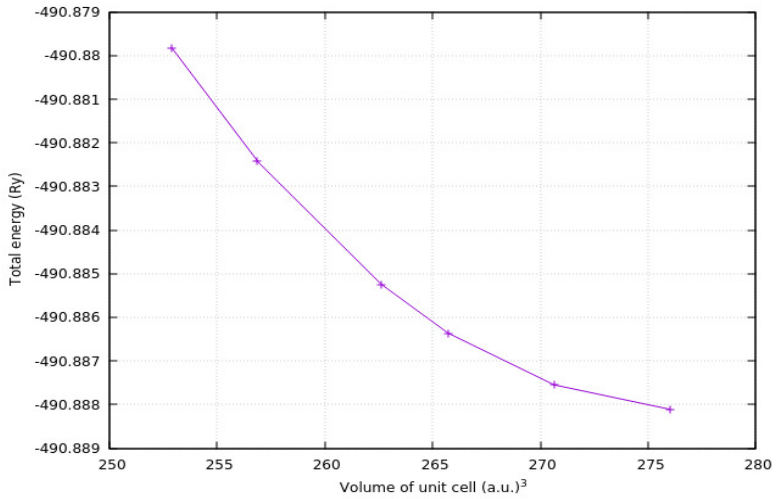

Figure 4. Indicates the variation of total energy (Ry) of α TiZr SMA with the volume of the unit cell under pressure up to 10GPa.

It is clear that there exists an inverse relationship between compression of a material and its lattice parameter. From the figure 3, we observed volume of unit cell $(a.u)^3$ decreases as the external pressure is applied and the smaller the lattice parameter, the smaller the volume and hence a large bulk modulus (Sifuna *et al*., 2017). This implies that bulk materials have a high resistance against volume deformation. In Figure 2, variations of the lattice parameters of α-TiZr Shape Memory Alloy with pressure are presented to investigate the influence of external pressure on the crystal structure of α-TiZr Shape Memory Alloy. It is observed that the lattice constants decrease with increase in external pressure. This is due to reduction of distance between the atoms as a result of pressure increase hence the repulsive interaction between atoms strengthens, leading to the difficulty to compress the crystal (Zhao *et al*., 2015). Figure 4 shows minimum total energy of α-TiZr Shape memory alloy at different pressure, we observe that minimum energy of the ground state increases with pressure. This is because when external pressure is applied to unit cell of α-TiZr Shape memory alloy, the bond length shortens thus the strength of covalent bond increases. The stronger the covalent bond the higher the minimum energy for the ground state.

3.2 Mechanical properties

3.2.1 Elastic properties

When a crystal is subjected to deformation of a certain magnitude of strain (σ), the restoring forces appear to bring it to the equilibrium state (Manyali, 2018). These restoring forces can be described by the stress tensor. For a small strain (ε) deforming a material determined by Hooke's law; (Landau *et al*., 1959)

$$\sigma_{ij} = C_{ijkl}\varepsilon_{ij} \qquad (2)$$

C_{ijkl} represents the elastic constants. Hence, the elastic matrix of hexagonal system is given as:

$$\begin{pmatrix}\sigma_1\\ \sigma_2\\ \sigma_3\\ \tau_1\\ \tau_2\\ \tau_3\end{pmatrix}\begin{pmatrix}C_{11} & C_{12} & C_{13} & & & \\ & C_{11} & C_{13} & & & \\ & & C_{33} & & & \\ & & & C_{44} & & \\ & & & & C_{55} & \\ & & & & & C_{66}\end{pmatrix}\begin{pmatrix}\varepsilon_1\\ \varepsilon_2\\ \varepsilon_3\\ \gamma_1\\ \gamma_2\\ \gamma_3\end{pmatrix} \quad (3)$$

where $\sigma_i, \tau_i, \varepsilon_i, \gamma_i$ are normal stress, shear stress, the corresponding normal strain and shearing strain respectively. In the current work elastic constants that were calculated for α-TiZr shape memory alloy under pressure up to 10GPa are presented in the table 2.The elastic properties such as the bulk modulus B, shear modulus G, Young's modulus E and Poisson's ratio are directly calculated by the Voigt-Reuss-Hill method (Hill, 1952). The results are listed in Table 2 and shown in Figure 6 and 7.

$$B_V = \frac{2C_{11}+2C_{12}+4C_{13}+C_{33}}{9} \quad (4)$$

$$B_R - \frac{(C_{11}+C_{12})C_{33}-2C_{13}^2}{C_{11}+C_{12}-4C_{13}+2C_{33}} \quad (5)$$

The Voigt average shear modulus is determined by the equation; (Voigt, 1928)

$$G_V = \frac{C_{11}+C_{12}-4C_{13}+2C_{33}+12C_{44}+12C_{66}}{30} \quad (6)$$

While Reuss average the shear modulus *(G)* is be given by the equation (Reuss, 1929)

$$G_R = \frac{5[(C_{11}+C_{12})C_{33}-2C_{13}^2]C_{44}C_{66}}{6B_V C_{44}C_{66}+2[(C_{11}+C_{12})C_{33}-2C_{13}^2](C_{44}+C_{66})} \quad (7)$$

From the Voigt-Reuss-Hill average, bulk modulus and shear modulus is expressed as;

$$B = \frac{B_V+B_R}{2} \quad (8)$$

$$G = \frac{G_V+G_R}{2} \quad (9)$$

A compound with a larger shear modulus implies its higher resistance to reversible deformations (Chen *et al*., 2014). Once the bulk and shear moduli are determined, Young's modulus (E) and Poisson's ratio ($\mathcal{V}$) are determined as shown below; (Greaves *et al*., 2011)

$$E = \frac{9BG}{3B+G} \quad (10)$$

$$V = \frac{3B-2G}{2(3B+G)} \quad (11)$$

Vicker's hardness H_v is associated with elastic properties of alloys. It denotes the resistance to elastic and plastic deformations when a force is loaded (Chang *et al*., 2018). Hardness can be predicted by the following equation; (Tian *et al*., 2012)

$$H_v = 0.92(G/B)^{1.137}G^{0.708} \quad (12)$$

3.2.2 Debye temperature ϑ_D and sound velocity V_m

The Debye temperature of a material is parameter associated with lattice vibrations used to describe the structural stability and the strength of bonds. It depends on the elastic constants and it is estimated from the average sound velocity V_m as shown; (Anderson, 1963)

$$\Theta_D = \frac{h}{k_B}\left(\frac{3n}{4\Pi V_a}\right)^{\frac{1}{3}} V_m \quad (13)$$

Where h is Plank's constant, k_B is Boltzmann's constant, n is number of atoms per formula unit and V_a is atomic volume.

The average sound velocity V_m ;

$$V_m = \left[\frac{1}{3}\left(\frac{1}{V_l^3} + \frac{2}{V_t^3}\right)\right]^{\frac{-1}{3}} \quad (14)$$

V_l is the longitudinal sound velocity and V_t is the transverse sound velocity of an isotropic aggregate determined as shown below;

$$V_l = \left(\frac{3B+4G}{3\rho}\right)^{\frac{1}{2}} \quad (15)$$

$$V_t = \left(\frac{G}{\rho}\right)^{\frac{1}{2}} \quad (16)$$

B is bulk modulus; G is the shear modulus and ρ is the density. By using the VRH method, average sound velocity and Debye temperatures with pressure range from 0 to 10 GPa is calculated and the results are listed in table 2.

Table 2. Mechanical properties and elastic constants for α-TiZr shape memory alloy under pressure up 10GP.

		Pressure (GPa)						Expt studies	Other studies
		0	2	4	6	8	10	0 (GPa)	0 (GPa)
C_{11} (GPa)		143.78	153.12	161.25	168.82	178.52	185.63	137.70	145.10
C_{12} (GPa)		64.55	69.46	74.12	75.09	83.35	87.14	75.30	72.50
C_{13} (GPa)		81.24	87.99	94.35	98.15	107.73	113.55	67.80	70.90
C_{33} (GPa)		144.30	155.69	165.84	169.86	189.29	194.14	164.00	169.00
C_{44} (GPa)		30.34	30.44	30.34	30.02	29.40	28.63	30.00	30.00
C_{66} (GPa)		39.61	41.83	43.56	46.86	47.58	49.24		
Θ_D (K)		297.30	301.57	304.21	307.47	308.18	308.33		
V- R-H (GPa)	B	98.4	105.60	112.30	116.36	126.21	132.00		
	E	90.83	93.46	95.97	98.65	100.30	101.28		
	G	33.73	34.55	35.34	36.30	36.67	36.91		
	V	0.346	0.352	0.357	0.358	0.367	0.372		
V_m(m/s)		2730.76	2751.91	2759.08	2777.68	2763.63	2750.76		
B/G		2.91	3.05	3.17	3.20	3.44	3.57		
H_v (GPa)		3.10	3.44	3.56	3.64	3.77	3.84		
Ref		This work						(ikehata *et al.*, 2004)	(Wang *et al.*, 2011)

 Available online http://ir.kabarak.ac.ke/handle/123456789/1

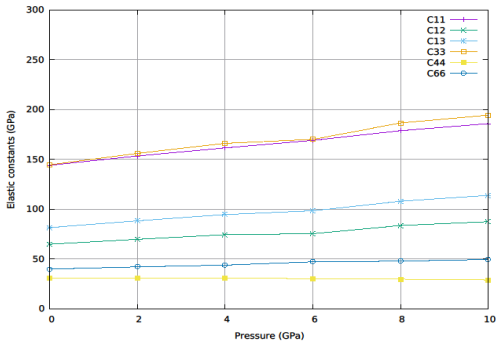

Figure 5. (Color online) Shows the pressure dependence of elastic constants in of α-TiZr SMA.

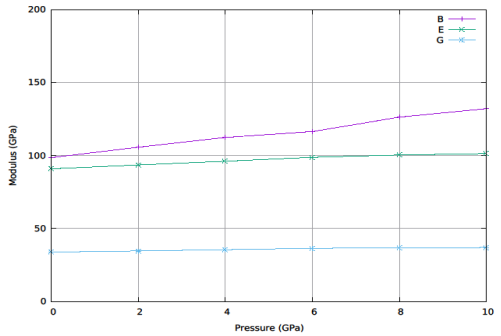

Figure 6. (Color online) Shows Bulk modulus, Young's modulus and shear modulus of α-TiZr memory shape alloy under pressure up to 10GPa.

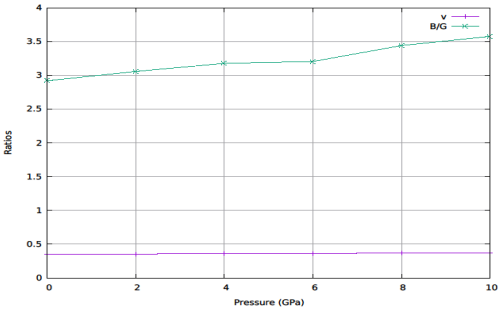

Figure 7. (Color online) Shows the poison's ratios and Pugh's ratios of α-TiZr SMA under pressure up to 10 GPa.

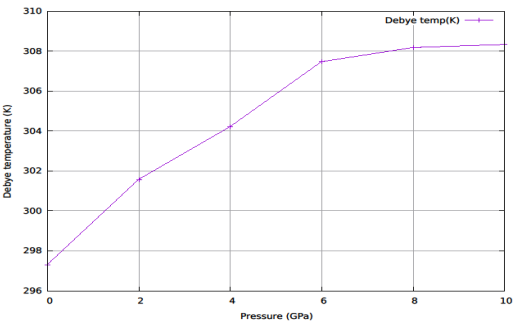

Figure 8. (Color online) Shows the Debye temperatures of α-TiZr SMA under varying pressure up to 10GPa.

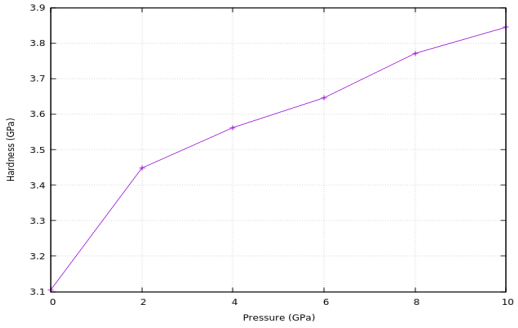

Figure 9. Hardness of α-TiZr memory alloy under pressure up to 10GPa

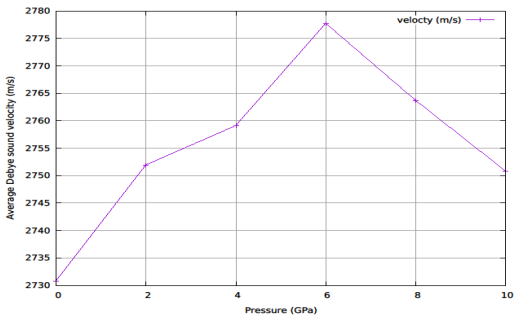

Figure 10. Shows the average Debye sound velocity of α-TiZr shape memory alloy under increasing pressure up to 10GPa.

 Available online http://ir.kabarak.ac.ke/handle/123456789/1

The stability in the hexagonal is based on the following conditions; (Born *et al*., 1954)

$$C_{11} > 0; 2C_{11}^2 < C_{33}(C_{11} + C_{11});\ C_{11} > 0;\ C_{66} > 0 \qquad (17)$$

Therefore, α-TiZr shape memory alloy is mechanically stable under external pressures between 0GPa to 10GP.

3.2.1 Pressure-Dependency of Elasticity

The information about elasticity under pressure helps us to understand the deformation behavior of a solid in response to external forces. In addition, the information provides a deeper insight into macroscopic mechanical behavior and estimate the hardness of materials (Chang *et al*., 2018). The calculated elastic constants are in good agreement with other studies as shown in table 2. The elastic constants C_{11} and C_{33} represent the elasticity in length. The other constants C_{12} and C_{44} are shear constants and are associated with the elasticity in shape. (Liu *et al*., 2012) It is evident that the elastic constants C_{11}, C_{12}, C_{13}, C_{33} and C_{66} of α-TiZr SMA increase linearly with pressure due to the denser packing of the atoms brought about by compression. The constants C_{11} and C_{33} are more sensitive to pressure compared to C_{12} and C_{13}, while C_{44} decreases slightly with pressure. We also noted that the elastic constant C_{11} is slightly smaller than C_{33} at the same pressure, therefore, it is easier to compress along the x-direction than along the z-direction.

Both Poisson's ratio ($\mathcal{V}$) and Pugh's ratio (B⁄G) are used to determine if the compounds are ductile or brittle for instance if v>0.26 (Greaves *et al*., 2011) or B⁄G>1.75 (Pugh's 1954) indicates that the crystal structure is ductile, otherwise brittle. From the Table 2 we realized that Pugh's ratios of α-TiZr shape memory alloy are greater than 1.75, thus this alloy is ductile. The ratios increase with pressure due to the strengthening of covalent bond, which suggests that higher pressure can improve the ductility as shown in Figure7. Poisson's ratio measures the stability of the crystal against shear, and the larger the Poisson's ratio, the better the plasticity (Cao *et al*., 2013). It is clear that the Poisson's ratio of α-TiZr shape memory alloy increases with pressure. Therefore, presence of an external pressure improves the plasticity α-TiZr shape memory alloy.

The values of bulk modulus from the Figure 6 are much greater than that of shear modulus, thus α-TiZr alloy tends to resist volume change better than shape change (Pugh, 1954). Young's modulus E shows the stiffness of a solid, for instance the materials with larger E are stiffer (Liu *et al*., 2013). Therefore, α-TiZr shape memory alloy becomes much stiffer when pressure increases. Moreover, it can be seen that values of B, G and E increase with pressure. This is because applied external pressure reduces the bond length hence the bond between Ti and Zr becomes stronger.

3.2.2 Pressure dependency of Vicker's Hardness in α-TiZr SMA

Our calculated value of Vicker's hardness indicated in table 2 lie between 3-4GPa suggesting that the α-TiZr SMA is soft. The Vicker's hardness increases with pressure as shown in Figure 9 due to increase in the strength of covalent bonds with external pressure. It is also noted that the shear modulus of materials plays a more important role in hardness than the bulk modulus of materials.

3.2.3 Pressure dependency of Debye temperature and sound velocity in α-TiZr SMA

Debye temperature is the temperature at which almost all modes of vibrations in a solid are excited (Bhatli *et al*., 1986). We found out that the Debye temperature of α-TiZr shape memory alloy increases with pressure which implies that the rigidity of the α-TiZr shape memory alloy increases with pressure as shown in Figure 8. Debye temperature is used to describe the strength of the covalent bond for instance the larger the Debye temperature the stronger the covalent bond (Liu *et al*., 2013). Therefore, with increase in external pressure, the covalent bonds of α-TiZr shape memory alloy become stronger.

Average sound velocity in α-TiZr SMA increase nonlinearly with pressure up to 6GPa and drops monotonically with further increase in pressure as shown in table 2 and Figure 10. Vibration frequency increases with pressure however, when external pressure increases beyond 6GPa, frequency decreases. This indicates that the bonds between the Ti and Zr atoms are strengthened as the distance between these two atoms becomes shorter with increasing pressure. The average sound velocity is determined from longitudinal sound velocity and transverse sound velocity which are related to elastic constants C_{11} and C_{44} using equations; $V_l = \sqrt{C_{11}/\rho}$ and $V_t = \sqrt{C_{44}/\rho}$ respectively. Longitudinal wave of compression depends on C_{11} while transverse wave is controlled by C_{44}. Therefore, transverse sound velocity of α-TiZr shape memory alloy increases while longitudinal sound velocity decreases under pressure. Normally $C_{11}>C_{44}$ hence , $V_l > V_t$ (Anderson, 1963).

Conclusions

In this paper, we have investigated the elasticity of α-TiZr shape memory alloy under various pressures up to 10GPa at a constant temperature 0K using Density Functional Theory. In our conclusion we realized the following; the obtained lattice constant of of α-TiZr shape memory alloy (3.07 Å) at 0 GPa is in good agreement with experimental and other theoretical values. Secondly, calculated elastic constants satisfies Born's stability criterion, therefore, α-TiZr Shape Memory Alloy is mechanically stable under pressure between 0GPa to 10GPa. Generally, elasticity of α-TiZr Shape Memory Alloy improves with increase in external pressure. In our research we focused on pressure dependency of elasticity in the α-TiZr Shape Memory Alloy at constant temperature however, temperature change may also cause cracks in buildings and bridges because of expansion and contraction. Therefore, further studies are necessary to understand the temperature dependent behaviors of α-TiZr shape memory alloy.

Acknowledgement

The authors acknowledge the Center for High Performance Computing (CHPC), South Africa for providing computational resources. Secondly, we appreciate Computational and Theoretical physics group (CTheP), Kenya for their discussions during their workshops. Lastly the authors extend thanks to the Department of Science, Technology and Engineering, Kibabii University, Kenya for providing the platform to carry out this research.

References

Anderson O.L., J. (1963). Phys. Chem. *Solids, 24,* 909.

Baloyi, M. E., Modiba, R., Chauke, H.R., and Ngoepe, P.E., (2018) IOP Conf. Ser.: *Mater. Sci.* Eng. 430 01202.

Bhatli, S. S., and Singh, S. T., (1986). J. Pure Appl. *Ultrasound. 8*, 1019 .

Bashkin, I.O., Fedotov, V.K., Nefedova, M.V., Tissen, V.G., Ponyatovsky, E.G., Schiwek, A., Holzapfel, W.B., (2003) Phys. *Rev. B* (68) 054401.

Birch, F., (1947). Phys. *Rev*. 71:809.

Born, M., and Kun, H., (1954). *Dynamical theory of crys-tal*, Clarendon press.

Cao, Y. Zhu, J.C. Liu, Y. Nong, Z.S. Lai, Z.H., (2013). Comp. Mater. *Sci. 69* 40.

Chancellor, N.B., Eatherton, M.R., Roke, D.A., and Akbaş, T., (2014). *Self-centering seismic lateral force resisting systems: High performance structures for the city of tomorrow. Buildings 4(*3): 520–548.

Chang, J., Zhou, X., Liu, K., Ge, N., (2018). R. Soc. open sci. *Struc tural, elastic, mechanical and thermodynamic properties of HfB4 under high pressure*. 5: 180701.

Chang, W. and Araki, Y. (2016). civil Engineering. *Use of shape-memory alloys in construction: a critical review;* (169): issue (CE2).

Chen, D.; Chen, Z.; Wu, Y.; Wang, M.; Ma, N.; Wang, H. (2014). Comput. Mater. Sci. *First-principles investigation of mechanical, electronic and optical properties of Al_3Sc intermetallic compound under pressure.* (91): 165–172.

Corso, D.A. (2016) J. Phys.: *Condens. Matter, 28,* 07540.

Giannozzi, P., Baroni, S., Bonini, N., Calandra, M., Car, R., Cavazzoni, C., Ceresoli, D., Chiarotti, G., Cococcioni, G., Dabo, I., *et al*., (2017). Journal of Physics: *Condensed Matter, 29,* 465901.

Greaves, G.N.; Greer, A.L.; Lakes, R.S.; Rouxel, T. (2011). Nat. Mater. *Poisson's ratio and modern materials*.10, 823–837. K, 1954.

Hill, R., (1952). Phys. Soc. Lond. Sect. *The Elastic Behaviour of a Crystalline Aggregate*. *A*, (65) 349–354

Ho, W.F. Chen, S.C. Wu, H.C. Hsu, (2008) J. Mater. *Med. 19*, 3179

Ikehata, H., Nagasako, N., Furuta, T., Fukumoto, A., Miwa, K., Saito, T., (2004). Phys. *Rev. B* (70) 174113.

Kohn, W., Sham, L. J., (1965). Phys. *Rev. 140* (4A) A1133–A1138.

Landau, L. D., and Lifshits, E. M. (1959). *Theory of elasticity (Translated from the Russian by J.B. Sykes and W.H. Reid)*. Addison-Wesley physics books. London, Pergamon Press; Reading, Mass., Addison-Wesley Pub. Co.

Li, Y., Cui, Y., Zhang, F and Xu, H. (2011). */ Scripta Materialia* (64): 584–587.

Liu, Y., Hu, W.C., Li, D.J., Zeng, X.Q., Xu, C.S., (2013). *Phys. Scr.* 88, 045302.

Liu, Y., Hu, W.C., Li, D.J., Zeng, X.Q., Xu, C.S., Yang, X.J. (2012). *Intermetallic,* 31, 257-263.

Manyali G.S., (2018) *High bulk modulus but low Vicker's hardness: A DFT study of mechanical properties of hcp rhenium, arXiv:* 1905.04526v1.

McNaught, A.D.; Wilkinson, A. (1997) *Compendium of Chemical Terminology.* In The Gold Book, 2nd ed.; Blackwell Scientific Publications: Oxford, UK,Volume 2, pp. 12–14, ISBN 0-86542-684-8.

Jani, M.J. Leary, M. Subic, A. Gibson, M.A. (2014). / *Materials and Design 56*, 1078–1113.

Monkhorst, H.J., Pack, J.D., (1976). *Phys. Rev. B* 13, 5188.

Perdew, J.P. Burke, K. Ernzerhof, M. (1996). Phys. Rev. *Lett. 77*, 3865.

Pugh, S.F., (1954). Philos. Mag. *Relations between the elastic moduli and the plastic properties of polycrystalline pure metals*, *XCII* 45, 823–843.

Reuss, A., (1929). Angew. Math. Mech. *Calculation of the flow limits of mixed crystals on the basis of the plasticity of monocrystals, Z,* (9): 49–58.

Sifuna, J., Manyali, G.S., Sakwa, T., Kitui, M.M., (2017) *Structural and Mechanical Properties of Bulk Scandium Trifluoride Investigated by First-Principles Calculations*; (4) 2; ISSN: 2458-9403

Soroushian, P., Ostowari, K., Nossoni, A and Chowdhury, H., (2015). Transportation Research Record. *Repair and strengthening of concrete structures through application of corrective posttensioning forces with shape-memory alloys.* 1770: 20–26. uly, Cambridge, UK.

Tian, Y.; Xu, B.; Zhao, Z. (2012). Int. J. Refract. Met. Hard Mater. *Microscopic theory of hardness and design of novel superhard crystals*, *33*, 93–106.

Voigt, W. (1928) Lehrbuchde Kristall. *physik*; B.G. Teubner: Leipzig/Berlin, Germany.

Wang, B.T., Li, W.D. and Zhang, P (2011). *First-principles calculations of phase transition, elasticity, and thermodynamic properties for TiZr alloy*, Beijing. China.

Zhao, Y., Qi, L., Jin, Y., Wang, K., Tian, J. and Han, P., (2015). */ Journal of Alloys and Compounds* 647, 1104e111.

Effects of solvent polarity on the absorption and fluorescence spectra of 3-cyano-7-hydroxy-4-methylcoumarin: Determination of the dipole moments and application to epifluorescence microscopy

Kebenei, J. Sellah[a] and Akumu E. Otieno[a*]
[a]Department of Physical and Biological Sciences. Kabarak University.
Private bag-20157
Kabarak
*Corresponding author: oakumu@kabarak.ac.ke

Abstract
The Absorption and fluorescence emission spectra of 3-cyano-7-hydroxy-4-methylcoumarin (3C7H4M) were studied in solvents of different dielectric constant ε and refractive index n. Experimental ground and excited state dipole moments were established by means of solvatochromic shift method. Both the ground state and excited state dipole moments were established. Results revealed that the excited state dipole moments of 3C7H4M were higher than those of the ground state. Further it is evident from these results that, the changes in the dipole moments on electronic excitation are small. Since 3C7H4M is more polar in its excited state, polar solvents were chosen in epifluorescence study. The epifluorescent microscopy images of a plant cell stained by 3C7H4M in various polar solvents compared with Iodine are hereby reported.

Keywords: 3-cyano-7-hydroxy-4-, *dipole moments, epifluorescence, spectral shifts*

Introduction

Photochemical studies on molecules typically requires knowledge of spectral features(Taniguchi & Lindsey, 2018). Fluorophores have unique electronic and photonic properties such as, relatively shorter lifetime, high quantum yield and broad spectral band width which can be applied in numerous technological applications (Raikar et al., 2006).

Coumarin dyes are well known photosensitizing agents(Zhang, Zhang, & Xia, 2008). They can be used in photobiology because of their photodynamic actions. They are known to show interesting photochemical behavior, particularly dimerization in polar and non-polar solvents (Perez-Rodriguez, Aguilera, & Figueroa, 2003).

The widespread occurrence of coumarin derivatives in nature (Kirsch, Abdelwahab, & Chaimbault, 2016) and their variety of applications have made their study very interesting. Dipole moments of short-lived species are of significant interest as they provide both electronic and geometrical structure information of the dye (Sharma, Jain, & Rastogi, 2007). The information on dipole moments of electronically excited species is helpful in the designing non-linear optical materials and understanding their photochemical transformations (Patil, Melavanki, Kapatkar, Ayachit, & Saravanan, 2011). Fluorescence experimental data on excited states are handy in the parameterization of semi-empirical quantum chemical procedures for these states (Grotkopp, Mayer, & Müller, 2018).

Determination of the ground and excited state dipole moments of dye molecules is important, because the values so obtained provide information about the change in electronic distribution upon excitation(Biradar, Siddlingeshwar, & Hanagodimath, 2008) The most popular technique for the determination of excited state dipole moments is based on the Lippert–Mataga equation (Vequi-Suplicy, Coutinho, & Lamy, 2014) in which absorption and fluorescence shifts described by dielectric constant ε and refractive index n are followed using the solvent polarity.

In this paper we report determination of dipole moments using different solvent parameters, refractive index, dielectric constant ε, spectral parameters like stokes shift. We have calculated

the ground and excited state dipole moments of 3C7H4M dye by solvent perturbation method based on absorption and fluorescence shift in solvents with varied polarities.

Theoretical

From the quantum mechanical perturbation theory of absorption($\tilde{\nu}_a$) and fluorescence ($\tilde{\nu}_f$) band shifts in different solvent permittivity (ε) and refractive index (η), the following equations (Nagaraja, Patil, Kusanur, Patil, & Melavanki, 2012), were used to determine both ground state and excited state dipole moments of the sample dye;

$$\tilde{\nu}_a - \tilde{\nu}_f = m_1 f(\varepsilon, n) + constant$$

and

$$\tilde{\nu}_a + \tilde{\nu}_f = m_2[f(\varepsilon, n) + 2g(n)] + constant$$

the solvent polarity parameter is given by;

$$f(\varepsilon, n) = \frac{2n^2+1}{n^2+2}\left[\frac{\varepsilon-1}{\varepsilon+2} - \frac{n^2-1}{n^2+2}\right]$$

and

$$g(n) = \frac{3}{2}\left[\frac{n^4-1}{(n^n+2)^2}\right]$$

with

$$m_1 = \frac{2(\mu_e-\mu_g)}{hca^3} \ldots\ldots\ldots\ldots\ldots\ldots\ldots (1)$$

and

$$m_2 = \frac{2(\mu_e^2-\mu_g^2)}{hca^3} \ldots\ldots\ldots\ldots\ldots\ldots\ldots (2)$$

Where *h* is the Planck's constant, *c* is the velocity of light in vacuum. μ_g and μ_e are the dipole moments in the ground and exacted states respectively which are calculated as follows;

$$\mu_g = \frac{m_2-m_1}{2}\left[\frac{hca^3}{2m_1}\right]^{\frac{1}{2}} \ldots\ldots\ldots\ldots\ldots (3)$$

$$\mu_e = \frac{m_2+m_1}{2}\left[\frac{hca^3}{2m_1}\right]^{\frac{1}{2}} \ldots\ldots\ldots\ldots\ldots (4)$$

The Onsager radius "*a*" of the solute molecule can be evaluated by using Edward's atomic increment method (Kadolkar, Patil, Kariduraganavar, & Inamdar, 2019) as follows;

$$a = \left[\frac{3M}{4\pi\delta N_A}\right]^{1/3}$$

Experimental

3C7H4M was purchased from Aldrich Chemical Co. and was used without further purification. The molecular structure of 3C7H4M is as given in Fig. 1. All the solvents used viz., methanol, ethanol, ethyl acetate, THF, and *n*-hexane, were of spectroscopic grade. Electronic absorption spectra were recorded on an Mrc UV-11 Model UV–Vis spectrophotometer. Fluorescence spectra were taken by using a Biobase-BKF93 Model F2000 fluorospectrometer at room temperature. Refractive index was measured using ATAGO model pocket refractometer PAL-1. Staining solutions of 3-cyano-7-hydroxy-4-methylcoumarin in water and methanol were prepared by dissolving 0.1 mg of the dye in 100 mL of distilled water (1 ppm). Iodine was prepared as per standard laboratory procedure. Each mixture was stirred for dye solubilization and filtered before use.

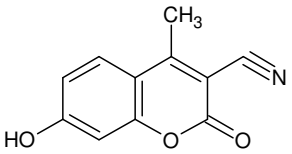

Fig.1. structure of 3-cyano-7-hydroxy-4-methylcoumarin

Results and discussion

Absorption and fluorescence emission spectra of 3-cyano-7-hydroxy-4-methylcoumarin (3C7H4M) and was recorded in solvents of different solvent parameters of dielectric constant ε and refractive index η. Figs. 2 and 3 show the absorption and fluorescence spectra of 3C7H4M respectively in solvents with various polarity indices as shown in table 1.

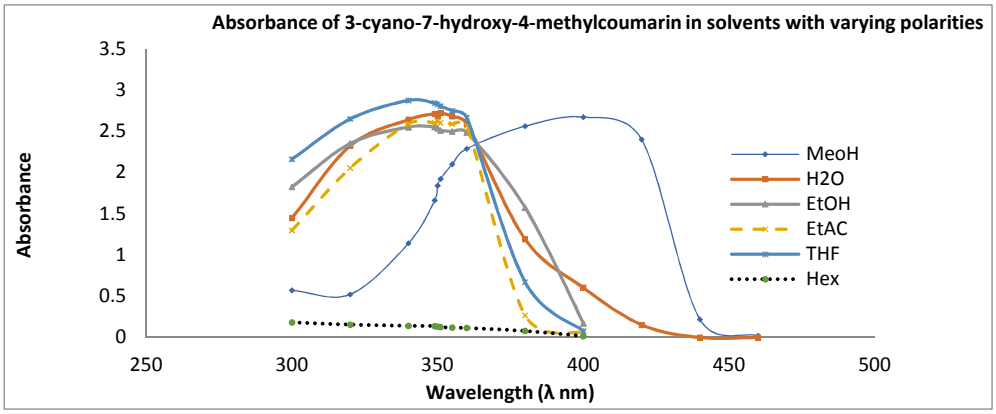

Fig.2. Absorption spectra of 3C7H4M in various solvents

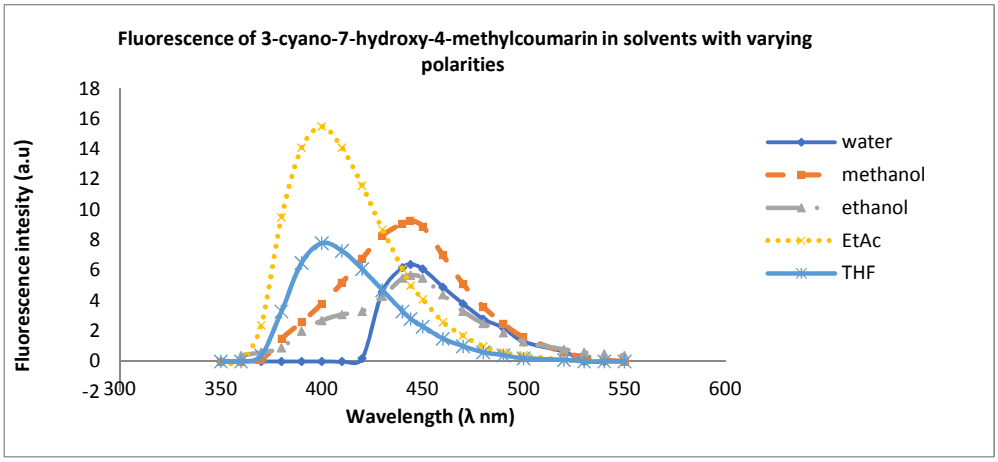

Fig3. Fluorescence spectra of 3C7H4M in various solvents.

 Available online http://ir.kabarak.ac.ke/handle/123456789/1

The absorption and emission spectra of 3C7H4M show maximum values around 340nm and 400nm respectively for THF, 350nm and 400nm respectively for ethyl acetate, 349nm and 444nm for ethanol respectively, 349nm and 440nm for methanol and 400nm and 444 for water.

However, the hexane solution did not show any absorbance and emission. This resulted in stokes shift ranging from 04–60nm on changing the solvent from water to THF and the emission spectra. The absorption and emission maxima, dielectric constant and refractive index of 3C7H4M in different solvents are given in Table 1.

Table 1.Solvent effects on the positions of absorption and fluorescence maxima

Solvent	**Polarity index**	**λ_{max} (Abs)**	**λ_{max} (Fluo)**	**(v_f - v_a)**	**ε**	**η**
THF	4.0	340nm	400nm	60nm	7.6	1.4120
Ethyl Ac	4.4	349nm	400nm	50nm	6	1.3681
Ethanol	5.2	400nm	444nm	44nm	24.3	1.3428
Methanol	6.6	408nm	440nm	32nm	32.7	1.3335
Water	10.2	440nm	444nm	4nm	78.4	1.3303

Table 1 cont.

	$\tilde{V}a$-$\tilde{V}f$ (cm^{-1})	**$\tilde{V}a$+$\tilde{V}f$(cm^{-1})**	**f(ε, η)**	**g(η)**	**f(ε, η)+2g(η)**
THF	-	-	0.4379	0.2793	0.9966
Ethyl Acetate	54411.76	4411.76	0.3866	0.2424	0.8715
Ethanol	25387.85	6131.18	0.6398	0.2219	1.0837
Methanol	51298.7	5844.16	0.6660	0.2145	1.0952
Water	47522.52	2477.48	0.7121	0.2120	1.1362

The charge transfer band shows a shift of about 08–100 nm in the absorption spectra on changing the solvent from THF to water and the emission spectra show smaller shift as compared with the absorption spectra. The highly pronounced absorption shift between water and other solvents implies that the ground state energy distribution is affected to a greater extent possibly due to the polar nature of 3C7H4M.

The magnitude of Stokes shift varies between from 04–160nm. The values of the Stokes shifts are also indicative of the charge transfer transition. On changing the solvent from a low polar, like THF to high polar like ethyl acetate shows a difference in Stokes shift of about 9nm again indicative of a charge transfer transition. The large magnitude of the Stokes shift indicates that the excited state geometry could be different from that of the ground state. The general observation is that there is an increase in the Stokes shift values with increasing solvent polarity which shows that there is an increase in the dipole moment on excitation.

Figs. 4 and 5 show the spectral shifts (in cm^{-1}) $\tilde{\nu}_a$- $\tilde{\nu}_f$ and $\tilde{\nu}_a$ + $\tilde{\nu}_f$ of 3C7H4M in polarity functions $f(\varepsilon, n)$ and$f(\varepsilon, n) + 2g(n)$. A linear progression was done data was fit to a straight line. The slopes m_1 and m_2 of the fitted lines shown in Figs. 4and 5.

 Available online http://ir.kabarak.ac.ke/handle/123456789/1

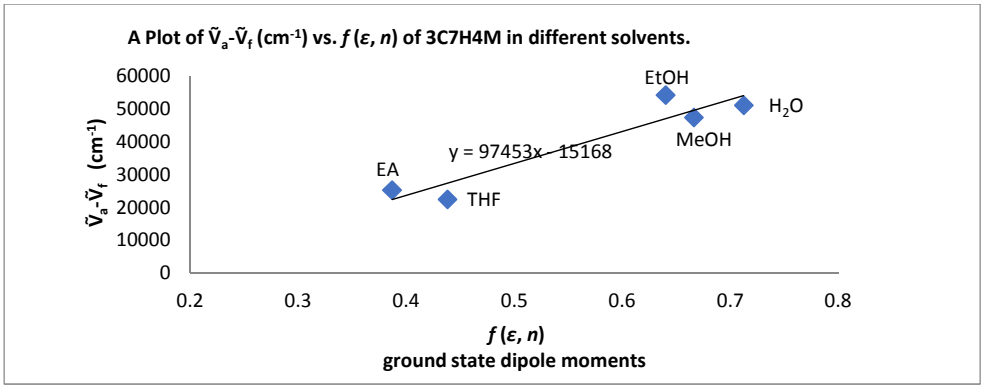

Fig.4. A Plot of $\tilde{V}_a$-$\tilde{V}_f$ (cm^{-1}) vs. $f(\varepsilon, n)$ of 3C7H4M in different solvents.

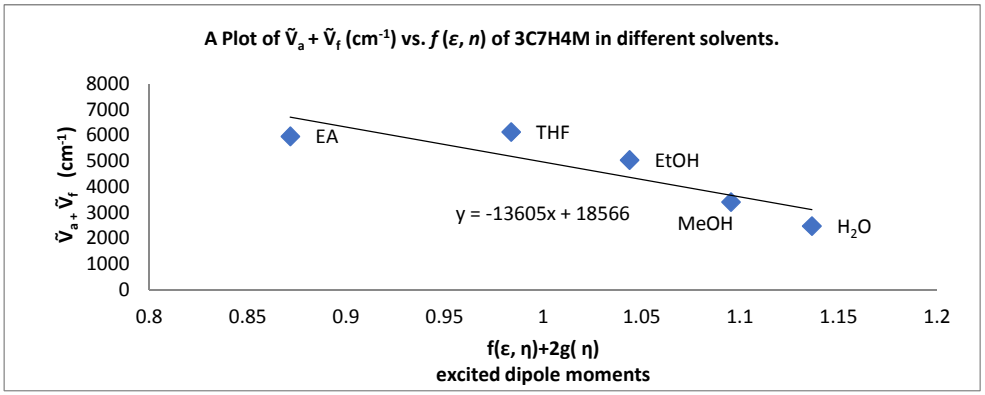

Fig.5. A Plot of $\tilde{V}_a + \tilde{V}_f$ (cm^{-1}) vs. $f(\varepsilon, n)$ of 3C7H4M in different solvents.

The slopes of Figs. 4 and 5 were found to be m_1 = 97453 cm^{-1} and m_2 = 13605 cm^{-1} and the Onsager radius (a) of solute was calculated using the equation;

$$a = \sqrt[3]{\frac{3M}{4\pi\rho N}} \simeq 3.8A$$

Where M is the molecular weight of the dye; ρ is the density of the dye; N is the Avogadro's number. We have approximated the density of this compound to be 1 g/mL. By using Eqs. (3) and (4), we get μg = 5.349 D and μe = 7.954 D and the change in the dipole moments ($\Delta\mu = \mu_g - \mu_e$) is 2.605 D. From Eqs. (3) and (4), the dipole moments μ_g and μ_e depends not only on m_1 and m_2 but also on radius of the solute. The linear dependence of spectral shifts on polarity function (Fig. 4 and 5) exhibits a good correlation. These experimental values were obtained in solution phase, where the solvent (matrix) is expected to introduce strong perturbation. Further it is evident from these results that, the changes in the dipole moments on electronic excitation are small.

Fig. 4 and 5 show images of epifluorescent microscopy of a plant cell stained by 3C7H4M in various polar solvents compared with Iodine. 3C7H4M stain in methanol almost compares with

the standard stain iodine. However, 3C7H4M in methanol appears to give brighter and clearer image of the cell. This is attributed to a higher fluorescence intensity of 3C7H4M in methanol unlike water and ammoniated water solutions.

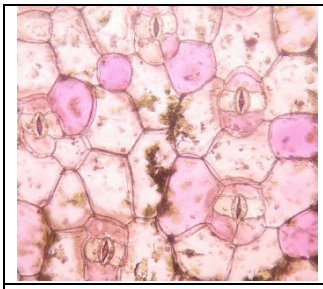	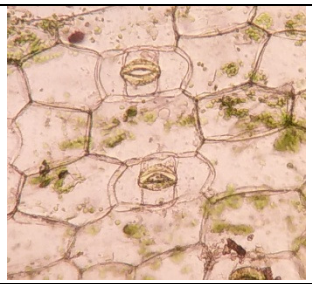	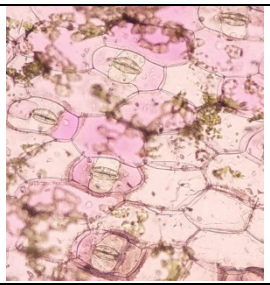	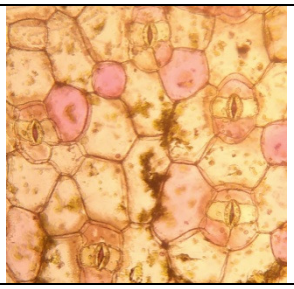
Methanol solvent	**Ammoniated water solvent**	**Water solvent**	**Iodine stain**

Fig.6. Images of living plant cells stained with 3C7H4M in various polar solvents compared with standard laboratory stain-Iodine viewed under a light microscope with resolution set at x10.

Conclusion

Both excitation and emission wavelengths of 3C7H4M in different solvents varying in polarity index has been determined. The Onsager radius has been calculated and the surface area of the molecule has been established, assuming the molecule as spherical and density is 1 g/mL. The determinations of dipole moments of C7H4M in the ground and excited states have shown that C7H4M is more polar in the excited state than the ground state. The results (fig.6) reveal that methanol is a better solvent for 3C7H4M in epifluorescence microscopy due to its polarity.

Conflict of interest statement

The authors declare that the research was conducted in the absence of any commercial or financial relationships that could be construed as a potential conflict of interest.

Acknowledgements

We cordially thank Kabarak University through the Directorate of Research for the financial support through this work.

References

Biradar, D. S., Siddlingeshwar, B., & Hanagodimath, S. M. (2008). Estimation of ground and excited state dipole moments of some laser dyes. *Journal of Molecular Structure*, *875*(1–3), 108–112. https://doi.org/10.1016/j.molstruc.2007.04.005

Grotkopp, O., Mayer, B., & Müller, T. J. J. (2018). Diversity-Oriented Synthesis and Optical Properties of Bichromophoric Pyrrole-Fluorophore Conjugates. *Frontiers in Chemistry*, *6*, 579. https://doi.org/10.3389/fchem.2018.00579

Kadolkar, P. S., Patil, S. A., Kariduraganavar, M. Y., & Inamdar, S. R. (2019). *Evaluation of ground and excited state dipole moments of alexa fluor 350-NHS ester in binary mixtures of DMSO-water*. 030029. https://doi.org/10.1063/1.5100456

Kirsch, G., Abdelwahab, A., & Chaimbault, P. (2016). Natural and Synthetic Coumarins with Effects on Inflammation. *Molecules*, *21*(10), 1322. https://doi.org/10.3390/molecules21101322

Nagaraja, D., Patil, N. R., Kusanur, R. A., Patil, H. D., & Melavanki, R. M. (2012). *Estimation of Ground and Excited State Dipole Moments of Coumarin Derivatives by Solvatochromic Method*. *2*(12), 9.

Patil, N. R., Melavanki, R. M., Kapatkar, S. B., Ayachit, N. H., & Saravanan, J. (2011). Solvent Effect on Absorption and Fluorescence Spectra of Three Biologically Active Carboxamides (C1, C2 and C3). Estimation of Ground and Excited State Dipole Moment from Solvatochromic Method Using Solvent Polarity Parameters. *Journal of Fluorescence*, *21*(3), 1213–1222. https://doi.org/10.1007/s10895-010-0800-4

Perez-Rodriguez, E., Aguilera, J., & Figueroa, F. L. (2003). Tissular localization of coumarins in the green alga Dasycladus vermicularis (Scopoli) Krasser: A photoprotective role? *Journal of Experimental Botany*, *54*(384), 1093–1100. https://doi.org/10.1093/jxb/erg111

Raikar, U. S., Renuka, C. G., Nadaf, Y. F., Mulimani, B. G., Karguppikar, A. M., & Soudagar, M. K. (2006). Solvent effects on the absorption and fluorescence spectra of coumarins 6 and 7 molecules: Determination of ground and excited state dipole moment. *Spectrochimica Acta Part A: Molecular and Biomolecular Spectroscopy*, *65*(3–4), 673–677. https://doi.org/10.1016/j.saa.2005.12.028

Sharma, N., Jain, S. K., & Rastogi, R. C. (2007). Solvatochromic study of excited state dipole moments of some biologically active indoles and tryptamines. *Spectrochimica Acta Part A: Molecular and Biomolecular Spectroscopy*, *66*(1), 171–176. https://doi.org/10.1016/j.saa.2006.02.039

Taniguchi, M., & Lindsey, J. S. (2018). Database of Absorption and Fluorescence Spectra of >300 Common Compounds for use in PhotochemCAD. *Photochemistry and Photobiology*, *94*(2), 290–327. https://doi.org/10.1111/php.12860

Vequi-Suplicy, C. C., Coutinho, K., & Lamy, M. T. (2014). Electric dipole moments of the fluorescent probes Prodan and Laurdan: Experimental and theoretical evaluations. *Biophysical Reviews*, *6*(1), 63–74. https://doi.org/10.1007/s12551-013-0129-8

Zhang, X., Zhang, J.-J., & Xia, Y.-Y. (2008). Molecular design of coumarin dyes with high efficiency in dye-sensitized solar cells. *Journal of Photochemistry and Photobiology A: Chemistry*, *194*(2–3), 167–172. https://doi.org/10.1016/j.jphotochem.2007.08.004